PNAS RESEARCH ARTICLE | NEUROSCIENCE

Regional variability in intracerebral properties of NREM to REM sleep transitions in humans

Laure Peter-Derex[a,b,1], Nicolás von Ellenrieder[c], Frank van Rosmalen[c], Jeffery Hall[c], François Dubeau[c], Jean Gotman[c], and Birgit Frauscher[c,d,1]

Edited by Yang Dan, University of California, Berkeley, CA; received January 12, 2023; accepted May 12, 2023

Transitions between wake and sleep states show a progressive pattern underpinned by local sleep regulation. In contrast, little evidence is available on non–rapid eye movement (NREM) to rapid eye movement (REM) sleep boundaries, considered as mainly reflecting subcortical regulation. Using polysomnography (PSG) combined with stereoelectroencephalography (SEEG) in humans undergoing epilepsy presurgical evaluation, we explored the dynamics of NREM-to-REM transitions. PSG was used to visually score transitions and identify REM sleep features. SEEG-based local transitions were determined automatically with a machine learning algorithm using features validated for automatic intra-cranial sleep scoring (10.5281/zenodo.7410501). We analyzed 2988 channel-transitions from 29 patients. The average transition time from all intracerebral channels to the first visually marked REM sleep epoch was 8 s ± 1 min 58 s, with a great heterogeneity between brain areas. Transitions were observed first in the lateral occipital cortex, preceding scalp transition by 1 min 57 s ± 2 min 14 s (d = −0.83), and close to the first sawtooth wave marker. Regions with late transitions were the inferior frontal and orbital gyri (1 min 1 s ± 2 min 1 s, d = 0.43, and 1 min 1 s ± 2 min 5 s, d = 0.43, after scalp transition). Intracranial transitions were earlier than scalp transitions as the night advanced (last sleep cycle, d = −0.81). We show a reproducible gradual pattern of REM sleep initiation, suggesting the involvement of cortical mechanisms of regulation. This provides clues for understanding oneiric experiences occurring at the NREM/REM boundary.

intracranial EEG | local sleep | rapid eye movements | sawtooth waves | atonia

Significance

Scalp electroencephalography (EEG) defines sleep globally, but stereo-EEG allows multilocal sleep scoring. We provide evidence that the non–rapid eye movement (NREM) to REM sleep transition is a progressive phenomenon underpinned by local cortical sleep regulation. We report a strong local heterogeneity as well as a reproducible and gradual pattern of REM sleep onset, suggesting that short- and long-term homeostasis differentially applies to brain areas. A key role is played by the occipital cortex, which exhibits the first cortical manifestations of REM sleep, on average 2 min before the scalp EEG detected transition. Further studies on the experiential correlates of local REM sleep may help to understand subjective oneiric and motor phenomena occurring at the boundary between NREM and REM sleep.

Vigilance states have traditionally been considered to be global homogeneous states, separated by clear-cut transitions, and regulated by subcortical networks (1). In contrast to this paradigm, research of the last years provided evidence that many sleep features are under local control and that sleep becomes global only when a large and widespread number of cortical regions are synchronously involved (2).

In the spatial domain, most sleep oscillations exhibit local specificities. Regarding non–rapid eye movement (NREM) sleep, several authors showed for instance that slow waves occur mostly locally, propagate from the frontal cortex to other regions, and that they are regulated locally by previous waking or cognitive activity (3–6). Spindles also present region-specific characteristics in terms of frequency and density and exhibit low synchrony across brain regions (7–9). During rapid eye movement (REM) sleep, local activities have been reported as well, such as electroencephalography (EEG) activation in the motor cortex during phasic REM sleep, theta waves in the posterior areas proposed to be the occipital part of ponto–geniculo–occipital waves, or sawtooth waves which were shown to exhibit high spatial heterogeneity (10–12).

In the temporal domain, boundaries between vigilance states appear more progressive and asynchronous between brain areas than previously thought (13). In humans, intracranial EEG studies demonstrated that sleep onset does not involve the whole brain simultaneously and that even during sleep, certain regions exhibit wake-like activity, while others are still asleep (14–18). Regarding sleep-to-wake transitions, functional imaging studies suggest that awakening is also a progressive process associated with sequential reactivation of brain structures underlying the sleep inertia phenomenon marked by decreased arousal level and temporary impaired performance upon awakening (19–21). These findings corroborate studies in rodents, showing the progressive restoration of a wake-like activity pattern after sleep offset in cortical neurons explored with microwire arrays (22). In contrast to this growing evidence regarding wakefulness and NREM sleep, little information is available regarding NREM to REM sleep transitions.

According to neurobiological models of sleep stages, the NREM to REM sleep transition depends mainly on brainstem structures showing abrupt changes in activity from one stage to another (23). However, some clinical situations suggest that NREM to REM sleep

Author contributions: L.P.-D., N.v.E., F.v.R., J.G., and B.F. designed research; L.P.-D., F.v.R., J.H., F.D., and B.F. performed research; N.v.E. contributed new reagents/analytic tools; L.P.-D., N.v.E., and B.F. analyzed data; and L.P.-D., N.v.E., F.v.R., J.H., F.D., J.G., and B.F. wrote the paper.

The authors declare no competing interest.

This article is a PNAS Direct Submission.

[1]To whom correspondence may be addressed. Email: Laure.peter-derex@chu-lyon.fr or Birgit.frauscher@mcgill.ca.

This article contains supporting information online at https://www.pnas.org/lookup/suppl/doi:10.1073/pnas.2300387120/-/DCSupplemental.

Published June 20, 2023.

transitions are not always clear-cut, giving rise to REM sleep parasomnias such as hypnagogic hallucinations or sleep paralysis (24, 25). Moreover, results from scalp EEG studies suggest that the mechanisms determining the occurrence of REM sleep periods gradually increase several minutes before REM onset, whereas those associated with NREM sleep decrease their activity only few seconds before REM sleep onset, leading to a progressive transition between NREM and REM sleep (26). The instability of NREM sleep during the ascending slope of NREM episodes, associated with a higher frequency and intensity of arousals, as well as a progressive decrease in delta and sigma activity and a progressive increase in alpha and high beta activities (27–29) may promote the gradual appearance of REM sleep features (sawtooth waves, muscle atonia, and bursts of REMs) during the NREM to REM sleep transition (30, 31).

Stereoencephalography (SEEG) recordings combined with polysomnography (PSG) feasible only in humans undergoing epilepsy presurgical evaluation provide the unique opportunity to investigate global/local sleep phenomena by enabling access to local activities of various brain areas including deep-seated regions with high spatiotemporal resolution. Recently, such recordings allowed to demonstrate that the hippocampus enters REM sleep before the neocortex in humans (32), thus confirming findings obtained in rodents (33, 34). This asynchrony may also apply to other brain areas; however, the study about hippocampo–neocortical dissociation in vigilance states relied on manual sleep scoring, which is not feasible for every local brain region. This methodological issue has so far prevented obtaining a global picture of local asynchronies during the NREM to REM sleep transition, although this is of great relevance for the understanding of sleep physiology and pathophysiology. Recently, we developed "SleepSEEG," an algorithm allowing to perform both global and local automatic sleep scoring using SEEG signals only, based on 24 features describing the oscillatory and nonoscillatory components of the signal spectrum and characteristics of sleep transients (35). In the present study, using the same method of SEEG analysis coupled with the visual scoring of REM sleep features on scalp EEG-PSG, we explored the dynamics of NREM to REM transitions with a multilocal approach. We investigated whether i) the REM sleep onset occurs simultaneously or asynchronously across different brain regions; ii) a reproducible anatomical pattern of NREM to REM transitions can be identified; and iii) regulating factors such as sleep homeostasis influence the dynamics of NREM to REM transitions. Based on earlier scalp EEG studies and on the concept of sleep as a local process (2), we hypothesized that the timing of the REM sleep onset might vary across the different brain areas but would follow a reproducible orchestration across subjects and would be modulated by sleep homeostasis.

Results

REM Sleep Features during Scalp NREM to REM Transitions. There were a total of 127 transitions marked on PSG nights in 29 patients (mean age 35.5 ± 10.6 y, range 18 to 44 y, 44.8% of women). One of these transitions was discarded since it was a W (instead of N1/N2/N3) to R transition (sixth and last transition of the night). Three more transitions from one patient were excluded due to proximity to seizures. This resulted in 123 NREM to REM transitions for analysis (28% N1 to R, 64% N2 to R, and 8% N3 to R transitions), including 123 REMs markers, 118 sawtooth waves markers, and 104 muscle atonia markers (Fig. 1*A*). In 71% of the transitions, sawtooth waves were the first features. They preceded the onset of muscle atonia by 2 min 44 s ± 2 min 45 s (average ± SD) and the first burst of REMs by 4 min 02 s ± 2 min 46 s. In 76% of the transitions, the onset of muscle atonia preceded the first burst of REMs. The onset of muscle atonia was 1 min 13 s ± 1 min 47 s before the first burst of REMs. The time between the first and last of the three markers was 4 min 12 s ± 2 min 35 s. Sawtooth waves appeared 4 min 04 s ± 2 min 39 s before the beginning of the first epoch scored as REM sleep, the muscle atonia 1 min 14 s ± 1 min 43 s, and the first burst of REMs 1 min ± 41 s (Fig. 1*A*).

Local Intracranial Transitions and Model Selection. No REM sleep (stage R) was detected by the automatic scoring in 151 channel × transitions (5.0% of all channel × transitions). The

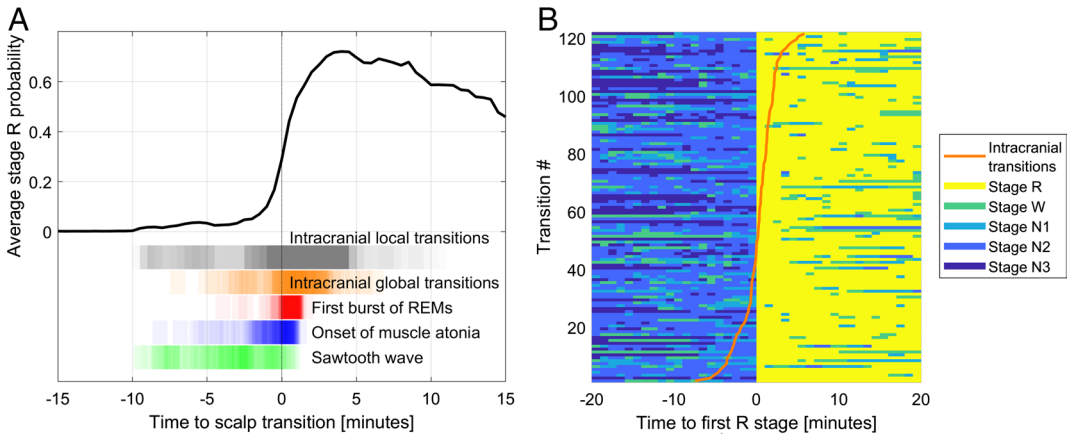

Fig. 1. Time course of NREM-to-REM transitions. (*A*) Time course of the intracranially scored stage R probability during transitions to REM sleep relative to the manually scored transition on PSG with scalp EEG. The black curve represents the average R-stage probability as a function of time in all (n = 2,837) transitions, with t = 0 being the onset of the first manually marked R epoch. Note that this curve shows a gradual increase before t = 0 and does not reach 1, as it is based on intracranial sleep scorings which exhibit transitions at various times and where transitions are calculated as probabilities of stage R. At the bottom of the figure, vertical black lines represent individual transitions as derived from each intracerebral channel, and vertical orange lines indicate the time of the global intracranial transitions averaging the channels of the corresponding patient after discounting the effect of the brain region. Vertical red lines represent the first burst of REMs, vertical blue lines the muscle atonia onset, and vertical green lines the first sawtooth wave burst. Note the overlap between these EOG/EMG/scalp EEG markers and some local intracranially scored NREM to REM transitions, several minutes before the scalp transition. (*B*) Time course of the 30-s epoch staging as a function of time in the 120 NREM to REM sleep transitions. The color indicates the manually scored scalp stages. The orange line shows, for each scalp transition, the timing of its associated global intracranial NREM to REM sleep transition. The global transitions are determined from all analyzed intracranial channels of the corresponding patient, discounting the effect of the relative delay of the different brain regions. The transitions have been ordered based on the time of the global intracranial transitions.

regions with undetected transitions significantly different from the 5.0% average (permutation test with Holm–Bonferroni correction for multiple comparisons) were the superior temporal gyrus with 17% (13/76), the posterior cingulate with 0.6% (1/163), and the lateral occipital lobe with 0% (0/124). This left 2,837 channel transitions (from 120 transitions, 718 channels, 29 patients) for subsequent analysis which focused on automatically scored intracranial local sleep stages at the transition to REM sleep. The average time of the transitions from all the intracerebral channels to the first PSG-marked R epoch was 8 s ± 1 min 58 s (Fig. 1*B*).

A model selection algorithm was used to explain the time difference between scalp and intracranial transitions with different variables (brain regions, patient, sleep cycle number, transition, and channels). The best model was the one including one variable for each transition and each brain region ($P < 0.0001$). These variables constitute the global transition times and brain region delays shown in the remainder of the *Results*. An example of the relationships between global manual scalp scoring, global intracranial automatic scoring, and local intracranial automatic scoring is provided in Fig. 2.

Characteristics of Intracranial Automatically Scored NREM to REM Transitions.

Clarity of transitions. We quantified the clarity of the transitions as the correlation coefficient between the probability of stage R reported by the automatic scoring algorithm and an ideal transition with null probability for 10 min before the actual transition and a probability of close to 1 for the subsequent 5 min (i.e., clear-cut stable transition). Fig. 3 shows an example of a clear and unclear transition (*SI Appendix*, Fig.S3). The clarity was highest for the posterior cingulate gyrus (0.85 ± 0.22, d = 0.34) and the mesiotemporal region (0.85 ± 0.20, d = 0.43) and lowest for the superior temporal gyrus (0.66 ± 0.26, d = 0.51), the planum temporale and transverse temporal gyrus (0.68 ± 0.24, d = 0.39), and the fusiform gyrus (0.68 ± 0.22, d = 0.39). The average clarity of the transitions for all the brain regions is shown in Fig. 4*A*.

Anatomical pattern of local transitions. The relative delay of the local transitions in each brain region is shown in Fig. 4*B*. Transitions were observed on average first in the lateral occipital cortex, preceding the scalp transition by 1 min 57 s ± 2 min 14 s (d = −0.83). Other regions with early transitions were the fusiform gyrus (1 min 45 s ± 3 min 19 s, d = −0.74) and mesial–occipital region (1 min 5 s ± 2 min 32 s, d = −0.46). Regions with late transitions were the triangular part of the inferior frontal gyrus and the anterior and lateral orbital gyri (1 min 1 s ± 2 min 1 s, d = 0.43, and 1 min 1 s ± 2 min 5 s, d = 0.43, after the scalp transition). The example in Fig. 3 corresponds to regions with early and late transitions (*SI Appendix*, Fig. S3). The region where the transition was the closest to the global scalp transition was the mesiotemporal

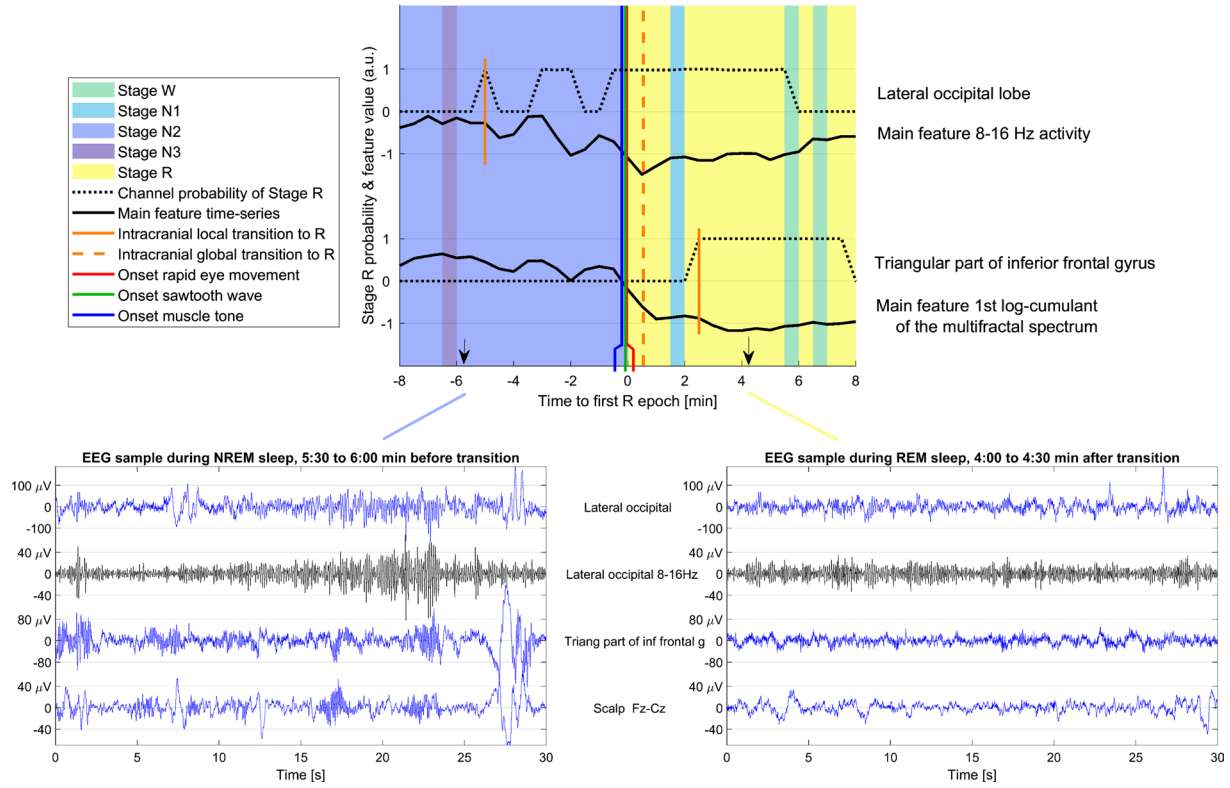

Fig. 2. Example of a transition between NREM and REM sleep and typical intracranial EEG in NREM and REM. (*Top*) Transition between NREM and REM sleep in patient 28, showing two channels in different brain regions. The background color indicates the sleep stage as scored by human experts. The black curves show the variation in time of the most important feature for determining the transition time in the corresponding brain region. The dotted black lines show the probability of NREM for each of the channels as a function of time. The first epoch with stage R in each intracerebral channel is indicated with a short vertical orange line, while the broken vertical orange line indicates the global transition time as derived from all the intracerebral channels used in this patient. The vertical green line indicates the onset of the first sawtooth waves, the vertical blue line the onset of muscle tone decrease, and the vertical red line the onset of the first rapid eye movements, all marked by human experts. In this example, the transition in the lateral occipital channel is observed 5 min before the scalp transition, and the transition in the triangular part of the inferior frontal gyrus is observed 3 min after the scalp transition. Note that the changes visually observed in the main features do not necessarily overlap with the first stage R local epoch because the transition in the channel is determined based on several features, and the threshold for determining the R stage depends on the values of the features during baseline NREM and R stages. (*Bottom*) Examples of the scalp EEG (Fz-Cz) and SEEG signals in one sleep epoch before and after the transition are shown on the bottom left and right. The same channels as in the top panel are shown. The blue traces correspond to the broadband signals and the black trace to the particular band associated with the most important feature in each brain region (8 to 16 Hz activity in the lateral occipital cortex, first log-cumulant of the multifractal spectrum in the triangular part of the inferior frontal gyrus, which in practice is highly correlated to the overall amplitude; thus in the latter case, the main feature corresponds to the raw blue signal). The amplitude scale is different to better show the signals in different channels, but it is the same in the NREM and REM epochs to facilitate the comparison.

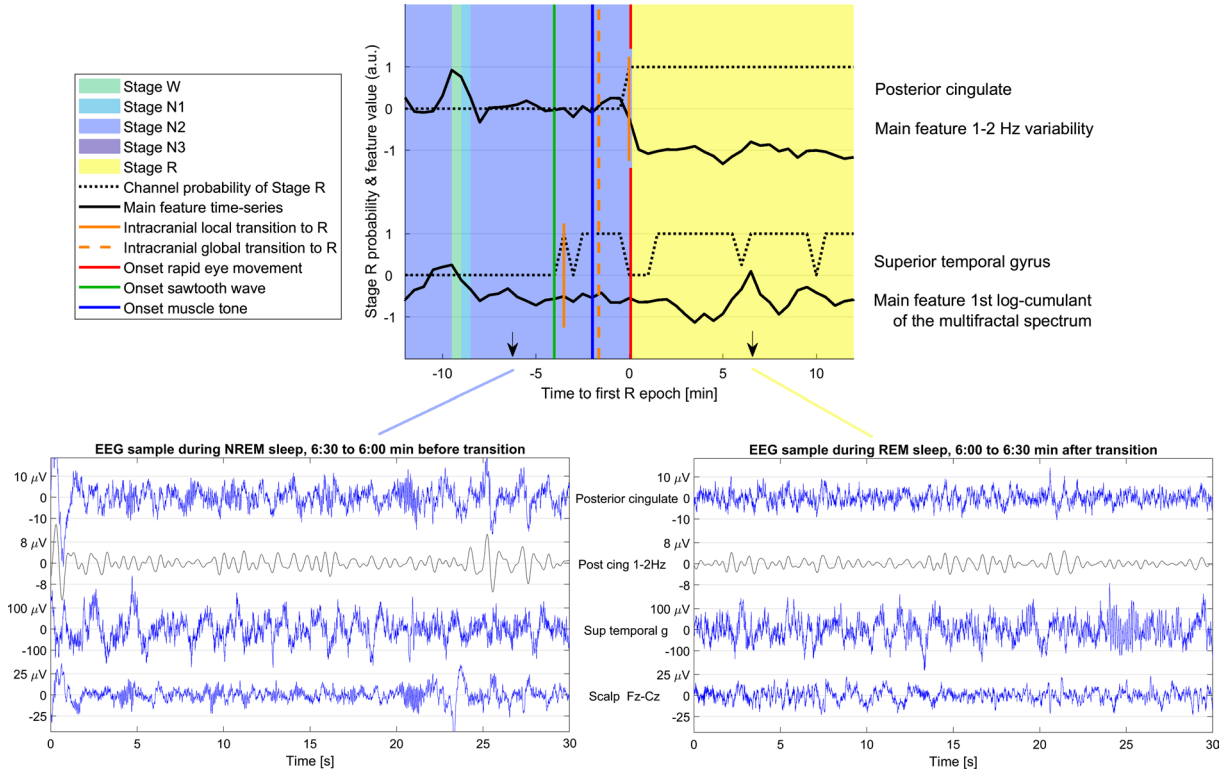

Fig. 3. Example of a transition between NREM and REM sleep and typical intracranial EEG in NREM and REM. (*Top*) Transition between NREM and REM sleep in patient 14, showing two channels in different brain regions. The background color indicates the sleep stage as scored by human experts. The black curves show the variation in time of the most important feature for determining the transition time in the corresponding brain region. The dotted black lines show the probability of NREM for each of the channels as a function of time. The first epoch with stage R in each intracerebral channel is indicated with a short vertical orange line, while the broken vertical orange line indicates the global transition time as derived from all the intracerebral channels used in this patient. Note that the transition in the channel is determined on several features, and the threshold for determining stage R depends on the values of the features during baseline NR and R sleep. In this case, changes are not visually observed in the main feature of the superior temporal gyrus. The vertical green line indicates the onset of the first sawtooth waves, the vertical blue line the onset of muscle tone decrease, and the vertical red line the onset of the first rapid eye movements, all marked by human experts. In this example, the transition in the posterior cingulate is a clear transition (high clarity), and the transition in the superior temporal gyrus is not clear (low clarity). (*Bottom*) Examples of the scalp EEG (Fz-Cz) and SEEG signals in one sleep epoch before and after the transition are shown on the bottom left and right respectively. The same channels as in the top panel are shown. The blue traces correspond to the broadband signals and the black trace to the particular band associated with the most important feature in each brain region (variability in the 1 to 2 Hz band activity in the posterior cingulate, first log-cumulant of the multifractal spectrum in the superior temporal gyrus, which in practice is highly correlated to the overall amplitude; thus in the latter case, the main feature corresponds to the raw blue signal). The amplitude scale is different to better show the signals in different channels, but it is the same in the NREM and REM epochs to facilitate the comparison.

area (mean absolute delay 1 min 21 s ± 1 min 27 s), which was also the closest to the REMs marker (1 min 34 s ± 1 min 34 s) and to the loss of muscle tone marker (1 min 49 s ± 1 min 43 s), while the occipital lobe transition was closest to the sawtooth wave marker (3 min 29 s ± 2 min 29 s).

Sleep Instability during the Peritransition Period. The pretransition period was marked by NREM sleep instability as quantified by the stage shift index based on scalp scoring with a median of 0.60 (0 to 1.3) stage changes per min. The most stable stage in the 10 min preceding the transition (longest run of consecutive epochs) was W in 2.4% of the transitions, N1 in 11.4%, N2 in 64.2%, and N3 in 22.0% (Fig. 1). Most features showed intermediate values between NREM and REM sleep (*SI Appendix*, Fig. S5 *B–D*) preceding the transition, possibly reflecting a smooth transition between NREM and REM sleep or transient wake-like or REM-like activities. The only feature showing a noticeable transition more extreme than NREM and REM was the third log-cumulant of the multifractal spectrum (*SI Appendix*, Fig. S5*A*), with higher values during the transition than during stable wake, NREM sleep, or REM sleep being in keeping with a more complex EEG signal composition. Defining stable sleep as uninterrupted NREM epochs for 10 min before the transition and uninterrupted R epochs for 5 min after the transition, 63% of the transitions were preceded by stable NREM, and 62% were followed by stable REM sleep. Of all the transitions, 38% were preceded by stable NREM sleep and followed by stable REM sleep. Subanalyses of these transitions showed that times between markers and transitions varied by less than 10% of their SD, except for the time between the global intracranial transitions to the first R epoch, which changed from 8 s to −21 s, a 23% of the 126 s SD among transitions. The regions with the earliest and the latest transitions were the same as found with the global analysis. The percentage of transitions × channels in which the automatic scoring algorithm could not find an epoch with stage R was reduced from 5.0% to 3.5% (37/1060) ($P = 0.038$). The median clarity of the intracranial transitions increased from 0.85 to 0.91 ($P = 0.036$). Regarding the effect of the pretransition NREM sleep stage, we observed that in transitions from N1, local intracranial transitions happened earlier (mean −55 s instead of 8 s compared to the scalp transition, $P = 0.006$). No other statistically significant differences were found associated with the pretransition NREM sleep stage.

Regulation of Intracranial Automatically Scored NREM to REM Transitions: Effect of Sleep Cycle. In order to explore the impact of sleep homeostasis on the transitions, we computed the average clarity and delay (after discounting the brain region effect) of the global intracranial and scalp transition as a function of the sleep cycle (Fig. 5). Intracranial transitions

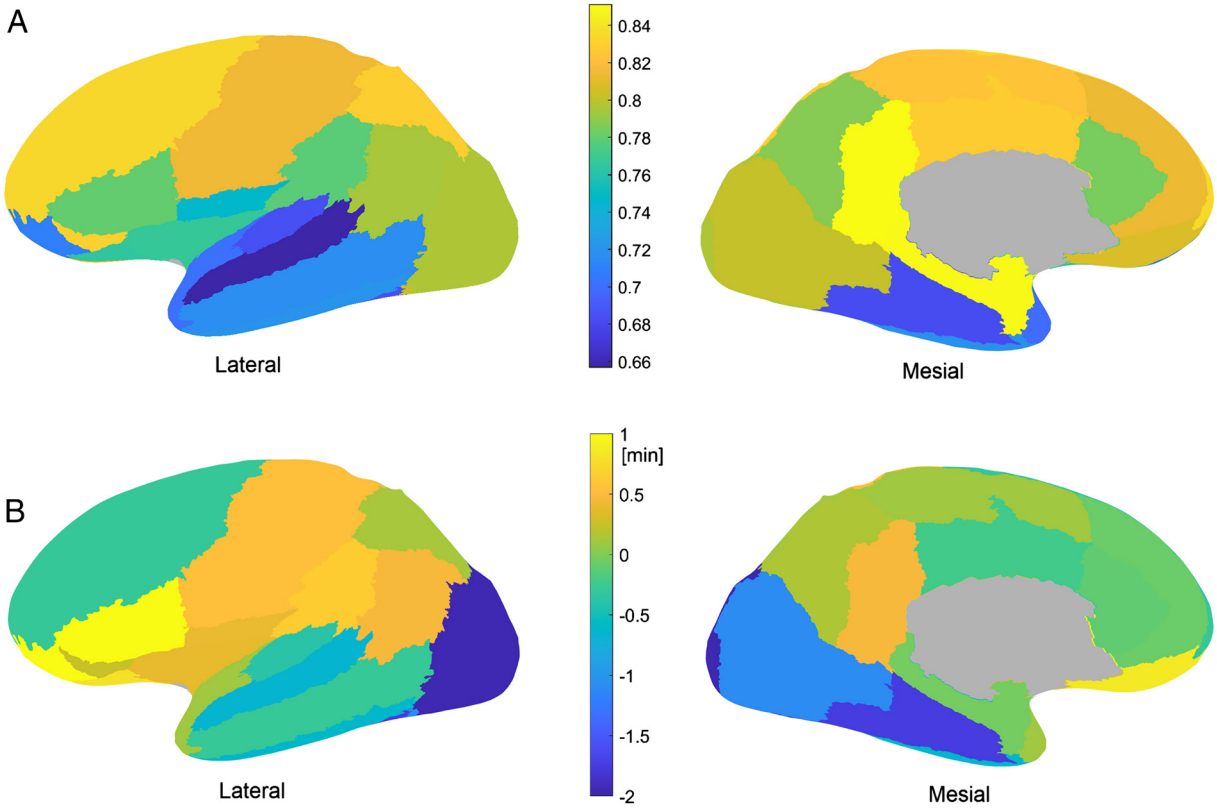

Fig. 4. Clarity and delay of the local NREM to REM sleep transition of different brain regions. (*A*) Clarity of the transitions. The clarity of the transition is highest in the posterior cingulate cortex and mesiotemporal regions and lowest in the rest of the temporal lobe. (*B*) Relative delay of the local transitions in different brain regions. On average, the transitions are observed in the lateral occipital cortex 3 min before the fronto-orbital cortex.

were less clear and earlier compared to the scalp as the night advances, without statistically significant regional differences. While the difference of clarity had small effect size for all cycles, the effect size of the delay was medium for the first (d = 0.47), second (d = 0.55), and fourth (d = −0.47) cycles and large (d = −0.81) for the fifth cycle.

Discussion

Using combined PSG-SEEG recordings and leveraging the complementarity of manual global scalp EEG and automatic local SEEG sleep scoring, we conducted a systematic study of local properties of NREM to REM sleep transitions. We demonstrated that i) the NREM to REM sleep transition is a progressive process underpinned by asynchronies between local brain regions transitions; ii) REM sleep onset shows a reproducible anatomical pattern starting in the occipital cortex and ending in the fronto-orbital cortex; and iii) this pattern is modulated by sleep homeostatic pressure.

A Gradual NREM to REM Sleep Transition as Assessed by REM Sleep Features. The sequential cascade of events initiated during NREM sleep before the onset of REM sleep is well known by sleep neurophysiologists used to detect sawtooth waves in the scalp EEG several minutes before REM onset. This is also consistent with the American Academy of Sleep Medicine sleep scoring guidelines, which do not consider sawtooth waves as a criterion for scoring REM sleep (36). Thus, a time lag of several minutes between the onset of the different REM sleep features was reported in PSG recordings (30); the majority of the time, the sequence of events

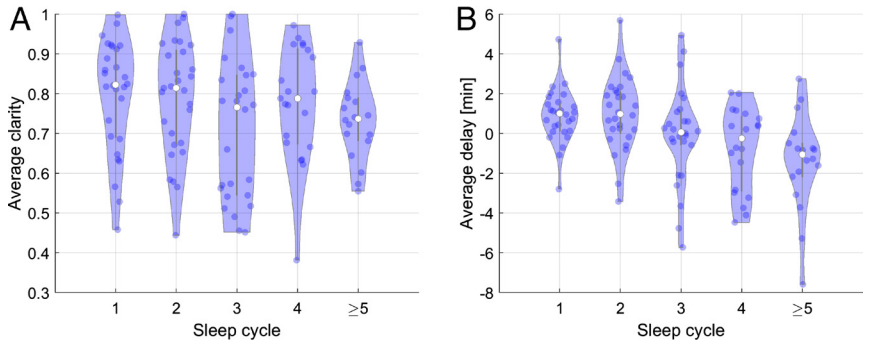

Fig. 5. Effect of sleep cycle on delay and clarity of transitions. (*A*) Clarity and (*B*) Delay between intracranial and scalp transitions with respect to the sleep cycle. Each dot represents a global transition. For later cycles, the clarity decreases and the intracranial transition occurs earlier, with the transition of the second cycle happening on average 1 min after the scalp transition and the fifth and later cycles 1 min 18 s before the scalp transition.

began with a reduction in muscle tone, followed by sawtooth waves appearance, and terminating with bursts of REMs. In our present work, we observed a different sequence, starting with sawtooth waves and then muscle atonia and bursts of REMs. This discrepancy might be linked to the duration of the time window used for the retrograde search of REM sleep features which was increased to up to 10 min in our study, allowing to capture earlier sawtooth wave bursts. We found a 4-min average delay between sawtooth waves and the first burst of REMs which was most often associated with the onset of REM sleep. This timing echoes a previous report of dramatic changes in scalp EEG in the 2 to 5 min preceding REM sleep onset as defined by the combination of EEG and non-EEG [electromyography (EMG) and electro-oculography (EOG)] criteria (26). Physiological mechanisms responsible for the generation of REM sleep features mainly involve brainstem structures. REM-on networks include glutamatergic neurons which drive muscle atonia and promote corticohippocampal activation, as well as cholinergic neurons which generate ponto–geniculo–occipital waves; REM-off mesencephalic GABAergic neurons, as well as noradrenergic and serotoninergic neurons, cease to inhibit REM-on neurons at the NREM to REM transition (1, 37). Complex interactions between these networks whose pattern of activity changes several minutes before stable entry into REM sleep (38) may account for the sequential appearance of REM sleep features.

Local Properties of NREM to REM Sleep Transitions. Our work adds to the understanding of the local properties of sleep, which until now had mainly been studied during sleep/wake transitions. On average, the transitions were observed in the lateral occipital cortex 3 min before the fronto-orbital cortex, although the time between the first and last local transition among all the explored intracranial channels reached 8 min. Local intracranial transitions happened earlier when the pretransition NREM sleep stage was N1, possibly reflecting the fact that N1 scoring in scalp was influenced by intracranial R. Transitions associated with more stable pre- and posttransition sleep were clearer, but there were no important differences in relative delays. The observed values are in the same order as those described in a recent paper on the hippocampo–neocortical sleep state divergence (32). In this paper, the authors compared manual scoring of sleep in the scalp EEG and in the hippocampus in eight patients explored with PSG-SEEG and found that nonsimultaneous state pairs, including REM in a structure and N2 in the other, had median durations of less than 2.5 min. Of note, in the Guthrie et al. study (32), the hippocampus was found to transition to REM before the cortex, whereas we observed in the present work that the mesiotemporal area exhibited the closest transition to the global scalp transition. This may be explained by the different (manual versus automatic) approach in local sleep scoring. Actually, no guidelines are available for hippocampus sleep stage scoring, and the specificities associated with sleep in this structure, such as a particular rhythmic slow (1.5 to 3 Hz) activity in REM sleep (39, 40), make the scoring rules used for scalp EEG difficult to apply (36). The strength of our study was the use of a validated automatic sleep scoring algorithm, which allowed not only to score a huge amount of data (29 nights in 718 channels) but also to overcome the issue associated with the heterogeneity of sleep patterns according to brain areas. This is particularly relevant for the lateral and inferior temporal cortex as well as the calcarine cortex, where sleep features exhibit specificities with lower rates of spindles and slow waves in NREM and lower beta as well as increased delta–theta activity in REM sleep as compared to the frontoparietal neocortex (41–44).

Regulations of NREM to REM Sleep Transitions. The heterogeneity in REM sleep onset may reflect differences in sleep regulation according to brain regions. Indeed, NREM sleep homeostatic pressure is higher in frontal regions and lower in occipital areas, where the decrease in slow wave activity over the night is also less pronounced (42, 45). This may account for the earlier entry of the occipital cortex into REM sleep which may in itself play an active role in the switching of sleep stages as recently reported in rodents (46). Interestingly, in this work, occipital activity was found to increase during the NREM to REM transition, immediately after the pontine part of the ponto–geniculo–occipital waves; this is in line with our observation of a close temporal relationship between sawtooth waves (believed to be the cortical component of ponto–geniculo–cortical waves) and REM sleep onset in the occipital cortex. We observed that the sleep cycle influenced the delay between the intracranial and the scalp EEG global transition, with the latest cycle showing an increased delay. The mechanisms underlying this cycle effect warrant further investigation. They may involve the dissipation the dissipation of NREM sleep pressure across the night and/or the short-term increase in REM sleep homeostatic pressure, thought to underpin ultradian sleep cycle regulation (47), and might be locally regulated.

Physiological and Pathophysiological Implications. Our findings not only provide insights about sleep physiology but also contribute to explain sleep-related experiences such as parasomnia occurring at the REM sleep borderland. Asynchrony in REM sleep onset may indeed translate into hallucinations (linked to the earlier entry of the occipital cortex in REM sleep) or sleep paralysis, which can be observed in pathological conditions like narcolepsy and are enhanced in case of sleep deprivation or in sleep/wake rhythms disorders when sleep regulation is challenged (24, 25). The presence of local REM sleep in global NREM sleep several minutes before the scored transition may also be associated with dreaming experiences and could represent the neurophysiological correlate of "covert REM" proposed to be responsible for much of the dream-like cognitive activity in NREM sleep (48). To note, dream reports are particularly prevalent during morning NREM sleep, which is in line with our finding of an increased delay between intracranial and scalp global transition, and thus a longer period of local REM sleep in NREM sleep (49, 50). Interestingly, reduced delta and increased beta–gamma frequency power was recently reported during the pre-REM period in people suffering from nightmares, suggesting an imbalance between sleep- and wake- or REM-promoting systems (51). The NREM-to-REM transition could thus be considered as a vulnerability period, likely to provide a biomarker of certain pathologies and to favor the emergence of undesirable experiences during sleep.

Limitations. We acknowledge several limitations. First, SEEG studies are always hampered by spatial sampling which does not provide homogeneous coverage of the brain, although we sought to overcome this bias by including a high number of patients. Second, results were obtained in patients with epilepsy under antiseizure medication, which is the only circumstance where these types of recordings are possible. However, channels with abnormal activity were carefully discarded from analyses, and results are in line with data obtained in animals, especially regarding the occipital cortex. Third, regional analyses (such as the homeostasis effect) were limited by the large variability of data resulting from limited numbers of events per region.

Fourth, the SleepSEEG algorithm provides information about sleep stage probability, which is a less clear-cut approach than

manual scoring, but aligns more with sleep physiology. The algorithm was built based on the scalp EEG sleep stage scoring, which may be a theoretical limit as local regions may be in different sleep stages than what is observed at the global scalp EEG scale and as local specificities were defined by the results of the classifier with a global to local approach. To note, only stable sleep periods excluding transitions were used to design the algorithm, and, in the test set, the global sleep stage derived from all channels staging using SleepSEEG showed high concordance with visual scoring for all sleep stages except N1 (35). Finally, SleepSEEG was not able to detect REM sleep in 5% of channels × transitions, mainly in the lateral temporal neocortex; this may be related to the clarity of transitions and to physiological specificities of sleep in these regions (41, 44).

Conclusion

In this study, we provide evidence that the transition from NREM to REM sleep is a reproducible and gradual process, spreading from the occipital to the frontal lobe with important local heterogeneity, thus reflecting local specificities in sleep regulation. Further work is needed to investigate the experiential correlates of this asynchrony and its modulation by pathological conditions.

Materials and Methods

Patient Selection. Charts of the 55 drug-resistant epilepsy patients who had undergone SEEG recordings combined with PSG including EOG and EMG of the chin and scalp EEG at the Montreal Neurological Institute and Hospital between September 2013 and September 2020 were reviewed. Inclusion criteria for the present study were i) age > 15, ii) presence of at least one intracranial EEG channel with normal activity, and iii) absence of secondarily generalized seizures during the 12 h before the evaluated sleep recording. Sleep cycles with focal symptomatic seizures were removed from the study, as well as NREM to REM transitions occurring from 10 min before to 10 min after focal asymptomatic epileptic discharges. Patients in whom epileptic activity, nonepileptic anomalies, or artifacts interfered with sleep scoring in the scalp EEG were excluded. The final study sample was composed of 29 patients. Information on the demographic and electroclinical findings of the investigated patient group is provided in *SI Appendix*, Table S1. This study was approved by the Review Ethics Board at the Montreal Neurological Institute and Hospital for the project "Insights into human REM sleep physiology: an intracerebral EEG study in epilepsy patients" (REB#MP-NEU-13-056). All patients granted written informed consent.

Intracranial and Scalp EEG Recording. An average of 10.3 (median 10, range 6 to 15) S-EEG Montreal Neurological Institute and Hospital (MNI) (10 contacts of 0.5 to 1 mm separated by 5 mm) or DIXI (10 to 15 contacts of 2 mm separated by 1.5 mm) depth electrodes were implanted stereotactically through an orthogonal or oblique approach using an image-guided system. Intracerebral electrode positions were tailored for each patient and depended on the clinical hypothesis. The deepest contacts were targeting the mesial aspect of the explored lobe, and the most superficial ones were targeting the lateral neocortex. The scalp EEG was obtained with subdermal thin wire electrodes at positions F3, F4, Fz, C3, C4, Cz, P3, P4, and Pz (52). On the night of the sleep recording, which was at least 72 h postimplantation, additional electrodes for EOG and chin EMG were applied. Sleep recordings started at around 20:00 and ended the next morning after spontaneous awakening. The median (range) time of "lights off" was 22:56 (20:42 to 2:08) and "lights on" was 7:39 (5:54 to 9:29), and the interval between these two markers was 8 h 38 m (6 h 44 m to 11 h 15 m). The EEG signal was high-pass filtered at 0.1 Hz, low-pass filtered at 500 Hz or 600 Hz, and sampled at 2 kHz. EEGs were recorded using the Harmonie EEG system (Stellate) from 2010 to 2017 and the NeuroWorkbench EEG system (Nihon, Kohden) after 2017. Recordings were acquired with a common reference (epidural electrode fixed in the bone). Scalp EEG analysis was performed using a standard bipolar montage (F3-C3; C3-P3; Fz-Cz; Cz-Pz; F4-C4; C4-P4) instead of a traditional mastoid referential montage because of the localization of the intracranial electrodes, the risk of infection as well as the potential contamination of this reference by epileptic activity in case of a temporal focus (9). All intracranial analyses were done using bipolar montages with the neighboring contacts on the S-EEG electrode in-depth EEG.

Selection of Intracranial EEG Channels. Only intracranial channels showing no or very rare epileptic discharges as well as no other background abnormalities and artifacts and that were not part of the seizure-onset zone were evaluated, as done in our previous work (12, 41, 53). Thus, we selected a total of 718 bipolar channels (median 16 per patient, range 3 to 105). The anatomic localization of electrodes was determined by coregistering preimplantation Magnetic Resonance Imaging (MRI) and postimplantation Computed Tomography (CT) or MRI of each subject, and individual coordinates were then standardized in a common stereotaxic space using minctools (http://bic-mni.github.io/) and the Intraoperative Brain Imaging System framework as previously described (53, 54). We joined the channels from both hemispheres and grouped the channels recording from the same brain region in 27 regions based on the Medical Image Computing and Computer Assisted Intervention (MICCAI) atlas (53, 55), with at least 10 channels from at least four patients in each region, except for mesiotemporal region with six channels from four patients. The template and the number of channels recording from each brain region are shown in *SI Appendix*, Figs. S1 and S2.

Visual Sleep Scoring. Sleep was scored manually in 30-s epochs of scalp EEG recordings in line with American Academy of Sleep Medicine criteria (36) by board-certified neurophysiologists (B.F. or L.P.-D.). All the NREM (N1, N2 or N3 stages) to REM transitions were marked by one of the scorers (B.F. or L.P.-D.), reviewed by the other, and, in case of disagreement, discussed to reach a consensus on the timing of the first REM epoch based on the available information gathered from EEG, EOG, and chin EMG. A transition was defined at the time of the first R epoch of each cycle, and only one (the first) transition per sleep cycle was kept. For each transition, we used the same consensus approach for the marking of i) the first burst of REMs (defined as a deflection <500 ms clearly standing out the background EOG); ii) the muscle atonia onset (defined as the first decrease in muscle tone amplitude so that it reached an amplitude no higher than in any other sleep stage, usually at the lowest level of the entire recording, for at least 1 s. For some transitions (~15%), the marking of muscle atonia was not possible because of already low muscle tone in NREM); and iii) the first burst of at least three consecutive sawtooth waves (defined as frontocentral surface positive 2 to 5 Hz waves of triangular morphology, with a slow incline to a negative peak with a consecutive steep linear decline ending in a positive peak as described in ref. 30). As clear sawtooth waves could be observed several minutes before some NREM to REM transitions, we decided to mark them up to 10 min prior to the transition.

Data Processing and Signal Analysis. SEEG-based local transitions were determined automatically by using a machine learning algorithm. The features were the same as in von Ellenrieder et al. (35) since they were deemed to be capable of very good performance in sleep scoring. The 24 spectral features are computed in 30-s epochs coinciding with the sleep scoring epochs and consist of three multifractal spectrum coefficients to characterize the nonoscillatory part of the spectrum, and 21 features derived from a wavelet decomposition of the data, including mean, SD, and sum of squares of the coefficients of seven scales related to the frequency bands of 0.5-1-2-4-8-16-32-64 Hz. Classification trees were used to perform a binary classification (stage R or another stage) for each channel and epochs in the interval between 10 min before and after each scalp transition. We defined the main feature for a brain region as the feature with highest average importance among all the channels in the region, where the importance of each feature is computed as the average risk in all splits of the classification tree nodes.

The training data corresponded to epochs from the same channel, from the whole night but away from any transition (at least 10 min away from any transition between stage R and other stages as scored on the scalp, except if there were less than 30 such epochs in stage R, in which case R epochs closer to the transitions were included until reaching 30). *SI Appendix*, Fig. S4*A* shows the degree to which each individual feature can separate the training data of stable R in different brain regions. Note, however, that the features are correlated, and a good separation for the individual feature does not mean high importance when using all features together to perform the classification. We defined the main feature for a brain region as the feature with highest average importance among all the channels in the region, where the importance of each feature is computed as the average risk in all splits of the classification tree nodes. The importance of different features

in different brain regions is shown in *SI Appendix*, Fig. S4*B*. Examples of average feature values around the transitions, used as the input to the classifier, are shown in *SI Appendix*, Fig. S5. The output of the classifier was the probability of stage R during the 20 min interval centered around each scalp transition (Fig. 2).

The transition time of the intracranial channel was determined as the start time of the first epoch in which the probability of stage R was higher than 0.5. Additionally, we defined the clarity of the transition as the correlation coefficient between the probability of stage R and an ideal transition with null stage R probability in the 10 min preceding the previously determined transition time, followed by 5 min of stage R probability equal to one. Thus, a clarity close to one would resemble an ideal transition, while if the stage R probability oscillates between low and high probability, the clarity would be low, indicating that there is not a large difference in the signal features between stage R and other stages.

Model Selection and Statistics. To aid in the interpretation of the channel/transitions data, we performed a model selection to explain the time difference data between scalp and intracranial transitions with different variables. We used the Akaike Information Criterion (AIC) with small sample size correction (56). The investigated variables were brain region, patient, sleep cycle number, transition number, and channel and all their valid combinations (some variables invalidate others, e.g., if there is a parameter for each channel, the brain regions cannot be assigned another parameter). The AIC selects a model minimizing a balance of the number of parameters (model complexity) and the residual error (quality of fit). The difference between AIC values for two models reflects the relative probability of the models and can be used to determine whether a model is significantly better than another (a difference in AICs higher than six implies the model with lower AIC value generated the data with a 95% probability).

Since we are not expecting that the transition characteristics are exactly the same in different brain regions, testing equality hypothesis is not informative. Instead, we focus on the effect size of the differences, which is of practical interest. We report the effect size via the Cohen's d value (d = 0.5 considered medium effect size, d = 0.8 large effect size) for time differences and via Cliff's d (d = 0.3 considered medium effect size, d = 0.5 large effect size) value for the non-normally distributed clarity measure.

Data, Materials, and Software Availability. All the data necessary for reproducing the results, all the results, and the code are publicly available at https://doi.org/10.5281/zenodo.7838640 (57). Raw data are available upon reasonable request to the senior author and in compliance with local ethical regulations.

ACKNOWLEDGMENTS. We wish to express our gratitude to the staff and technicians at the EEG Department of the Montreal Neurological Institute and Hospital, particularly Lorraine Allard, Nicole Drouin, and Chantal Lessard. This work was supported by the Natural Sciences and Engineering Research Council of Canada RGPIN2020-04127 and RGPAS-2020-00021 to B.F. B.F. was supported by Fonds de Recherche du Québec–Santé 2021-2025 Salary Award "Chercheur-boursier clinicien Senior."

Author affiliations: [a]Center for Sleep Medicine and Respiratory Diseases, Croix-Rousse Hospital, University Hospital of Lyon, Lyon 1 University, 69004 Lyon, France; [b]Lyon Neuroscience Research Center, CNRS UMR5292/INSERM U1028, Lyon 69000, France; [c]Montreal Neurological Institute and Hospital, McGill University, Montreal, QC H3A 2B4, Canada; and [d]Analytical Neurophysiology Lab, Montreal Neurological Institute and Hospital, McGill University, Montreal, QC H3A 2B4, Canada

1. C. B. Saper, P. M. Fuller, Wake-sleep circuitry: An overview. *Curr. Opin. Neurobiol.* **44**, 186–192 (2017).
2. J. M. Krueger *et al.*, Sleep as a fundamental property of neuronal assemblies. *Nat. Rev. Neurosci.* **9**, 910–919 (2008).
3. J. L. Cantero, M. Atienza, R. M. Salas, E. Dominguez-Marin, Effects of prolonged waking-auditory stimulation on electroencephalogram synchronization and cortical coherence during subsequent slow-wave sleep. *J. Neurosci.* **22**, 4702–4708 (2002).
4. R. Huber, M. F. Ghilardi, M. Massimini, G. Tononi, Local sleep and learning. *Nature* **430**, 78–81 (2004).
5. Y. Nir *et al.*, Regional slow waves and spindles in human sleep. *Neuron* **70**, 153–169 (2011).
6. V. Botella-Soler, M. Valderrama, B. Crepon, V. Navarro, M. Le Van Quyen, Large-scale cortical dynamics of sleep slow waves. *PLoS One* **7**, e30757. (2012).
7. T. Andrillon *et al.*, Sleep spindles in humans: insights from intracranial EEG and unit recordings. *J. Neurosci.* **31**, 17821–17834 (2011).
8. L. Peter-Derex, J.-C. Comte, F. Mauguiere, P. A. Salin, Density and frequency caudo-rostral gradients of sleep spindles recorded in the human cortex. *Sleep* **35**, 69–79 (2012).
9. B. Frauscher, N. von Ellenrieder, F. Dubeau, J. Gotman, Scalp spindles are associated with widespread intracranial activity with unexpectedly low synchrony. *Neuroimage* **105**, 1–12 (2015).
10. F. De Carli *et al.*, Activation of the motor cortex during phasic rapid eye movement sleep. *Ann. Neurol.* **79**, 326–330 (2016).
11. B. Frauscher *et al.*, Sharply contoured theta waves are the human correlate of ponto-geniculo-occipital waves in the primary visual cortex. *Clin. Neurophysiol.* **129**, 1526–1533 (2018).
12. B. Frauscher *et al.*, Rapid Eye Movement Sleep Sawtooth Waves Are Associated with Widespread Cortical Activations. *J. Neurosci.* **40**, 8900–8912 (2020).
13. S. Sarasso *et al.*, Fluid boundaries between wake and sleep: experimental evidence from Stereo-EEG recordings. *Arch Ital. Biol.* **152**, 169–177 (2014).
14. M. Magnin *et al.*, Thalamic deactivation at sleep onset precedes that of the cerebral cortex in humans. *Proc. Natl. Acad. Sci. U.S.A.* **107**, 3829–3833 (2010).
15. L. Nobili *et al.*, Dissociated wake-like and sleep-like electro-cortical activity during sleep. *NeuroImage* **58**, 612–619 (2011).
16. S. Sarasso *et al.*, Hippocampal sleep spindles preceding neocortical sleep onset in humans. *NeuroImage* **86**, 425–432 (2014).
17. L. Peter-Derex, M. Magnin, H. Bastuji, Heterogeneity of arousals in human sleep: A stereo-electroencephalographic study. *Neuroimage* **123**, 229–244 (2015).
18. P. Ruby, M. Eskinazi, R. Bouet, S. Rheims, L. Peter-Derex, *Dynamics of Hippocampus and Orbitofrontal Cortex Activity during Arousing Reactions from Sleep: An Intracranial Electro-Encephalographic Study* (Brain Mapp in press, Hum, 2021).
19. T. J. Balkin *et al.*, The process of awakening: A PET study of regional brain activity patterns mediating the re-establishment of alertness and consciousness. *Brain* **125**, 2308–2319 (2002).
20. R. Vallat, D. Meunier, A. Nicolas, P. Ruby, Hard to wake up? The cerebral correlates of sleep inertia assessed using combined behavioral EEG and fMRI measures. *Neuroimage* **184**, 266–278 (2019).
21. M. Ferrara *et al.*, The electroencephalographic substratum of the awakening. *Behav. Brain Res.* **167**, 237–244 (2006).
22. V. V. Vyazovskiy *et al.*, The dynamics of cortical neuronal activity in the first minutes after spontaneous awakening in rats and mice. *Sleep* **37**, 1337–1347 (2014).
23. J. Siegel, "REM sleep" in *Principles and Practice of Sleep Medicine*, R. T. Kryger MH, W. C. Dement, Eds. (Elsevier Saunders, ed. 5, St. Louis, MO, 2011), pp. 92–111.
24. M. M. Ohayon, R. G. Priest, M. Caulet, C. Guilleminault, Hypnagogic and hypnopompic hallucinations: Pathological phenomena? *Br. J. Psychiatry* **169**, 459–467 (1996).
25. A. Stefani, E. Holzknecht, B. Hogl, Clinical neurophysiology of REM parasomnias. *Handb Clin. Neurol.* **161**, 381–396 (2019).
26. R. Ferri *et al.*, Relationship between Delta, Sigma, Beta, and Gamma EEG bands at REM sleep onset and REM sleep end. *Clin. Neurophysiol.* **112**, 2046–2052 (2001).
27. P. Halasz, R. Bodizs, *Dynamic Structure of NREM Sleep* (Springer Science & Business Media, 2012).
28. H. Merica, R. D. Fortune, A neuronal transition probability model for the evolution of power in the sigma and delta frequency bands of sleep EEG. *Physiol. Behav.* **62**, 585–589 (1997).
29. S. M. McKinney, T. T. Dang-Vu, O. M. Buxton, J. M. Solet, J. M. Ellenbogen, Covert waking brain activity reveals instantaneous sleep depth. *PLoS One* **6**, e17351 (2011).
30. S. Sato *et al.*, Relationship between muscle tone changes, sawtooth waves and rapid eye movements during sleep. *Electroencephalogr. Clin. Neurophysiol.* **103**, 627–632 (1997).
31. K. Hadjiyannakis, R. D. Ogilvie, C. E. Alloway, C. Shapiro, FFT analysis of EEG during stage 2-to-REM transitions in narcoleptic patients and normal sleepers. *Electroencephalogr. Clin. Neurophysiol.* **103**, 543–553 (1997).
32. R. S. Guthrie, D. Ciliberti, E. A. Mankin, G. R. Poe, Recurrent Hippocampo-neocortical sleep-state divergence in humans. *Proc. Natl. Acad. Sci. U.S.A.* **119**, e2123427119 (2022).
33. J. J. Emrick, B. A. Gross, B. T. Riley, G. R. Poe, Different simultaneous sleep states in the hippocampus and neocortex. *Sleep* **39**, 2201–2209 (2016).
34. E. Duran, C. N. Oyanedel, N. Niethard, M. Inostroza, J. Born, Sleep stage dynamics in neocortex and hippocampus. *Sleep* **41** (2018).
35. N. von Ellenrieder, L. Peter-Derex, J. Gotman, B. Frauscher, SleepSEEG: Automatic sleep scoring using intracranial EEG recordings only. *J. Neural. Eng.* **19** (2022).
36. R. B. Berry *et al.*, *The AASM Manual for the Scoring of Sleep and Associated Events: Rules, Terminology and Technical Specifications, Version 2.4* (American Academy of Sleep Medicine, www.aasmnet.org, Darien, Illinois, 2017).
37. P.-H. Luppi *et al.*, Brainstem mechanisms of paradoxical (REM) sleep generation. *Pflugers Arch.* **463**, 43–52 (2012).
38. M. Steriade, S. Datta, D. Pare, G. Oakson, R. C. Curro Dossi, Neuronal activities in brain-stem cholinergic nuclei related to tonic activation processes in thalamocortical systems. *J. Neurosci.* **10**, 2541–2559 (1990).
39. R. Bodizs *et al.*, Rhythmic hippocampal slow oscillation characterizes REM sleep in humans. *Hippocampus* **11**, 747–753 (2001).
40. F. Moroni *et al.*, Sleep in the human hippocampus: A stereo-EEG study. *PLoS One* **2**, e867 (2007).
41. N. von Ellenrieder *et al.*, How the human brain sleeps: Direct cortical recordings of normal brain activity. *Ann. Neurol.* **87**, 289–301 (2020).
42. M. Gorgoni *et al.*, The distinctive sleep pattern of the human calcarine cortex: A stereo-electroencephalographic study. *Sleep* **44**, zsab026 (2021).
43. L. De Gennaro, M. Ferrara, G. Curcio, R. Cristiani, M. Bertini, Cortical EEG topography of REM onset: The posterior dominance of middle and high frequencies. *Clin. Neurophysiol.* **113**, 561–570 (2002).
44. L. Peter-Derex, N. V. Ellenrieder, B. Frauscher, "Physiological activity recorded with intracranial EEG: From wakefulness to sleep" in *A Practical Approach to Stereo EEG*, S. U. Schuele, Ed. (Springer Publishing Company, New York, 2020), pp. 303–314. 10.1891/9780826136930.0024.
45. V. Knoblauch, K. Krauchi, C. Renz, A. Wirz-Justice, C. Cajochen, Homeostatic control of slow-wave and spindle frequency activity during human sleep: Effect of differential sleep pressure and brain topography. *Cereb Cortex* **12**, 1092–1100 (2002).

46. Z. Wang *et al.*, REM sleep is associated with distinct global cortical dynamics and controlled by occipital cortex. *Nat. Commun.* **13**, 6896 (2022).
47. P. Franken, Long-term vs. short-term processes regulating REM sleep. *J. Sleep Res.* **11**, 17–28 (2002).
48. T. A. Nielsen, A review of mentation in REM and NREM sleep: "covert" REM sleep as a possible reconciliation of two opposing models. *Behav. Brain Sci.* **23**, 851–866; discussion 904–1121 (2000).
49. P. C. Cicogna, V. Natale, M. Occhionero, M. Bosinelli, A comparison of mental activity during sleep onset and morning awakening. *Sleep* **21**, 462–470 (1998).
50. S. L. Chellappa, C. Cajochen, Ultradian and circadian modulation of dream recall: EEG correlates and age effects. *Int. J. Psychophysiol.* **89**, 165–170 (2013).
51. B. Blaskovich, R. Reichardt, F. Gombos, V. I. Spoormaker, P. Simor, Cortical hyperarousal in NREM sleep normalizes from pre- to post- REM periods in individuals with frequent nightmares. *Sleep* **43**, zsz201 (2020).
52. J. R. Ives, New chronic EEG electrode for critical/intensive care unit monitoring. *J. Clin. Neurophysiol.* **22**, 119–123 (2005).
53. B. Frauscher *et al.*, Atlas of the normal intracranial electroencephalogram: neurophysiological awake activity in different cortical areas. *Brain* **141**, 1130–1144 (2018).
54. S. Drouin *et al.*, IBIS: An OR ready open-source platform for image-guided neurosurgery. *Int. J. Comput. Assist. Radiol. Surg.* **12**, 363–378 (2017).
55. B. Landman, S. Warfield, *2012 Workshop on Multi-Atlas Labeling* (Create Space Independant Publishing Plateform, 2012).
56. J. E. Cavanaugh, Unifying the derivations for the Akaike and corrected Akaike information criteria. *Stat. Probability Lett.* **33**, 201–208 (1997).
57. L. Peter-Dere *et al.*, Regional variability in intracerebral properties of NREM to REM *sleep* transitions in humans. *Zenodo*. https://zenodo.org/record/7838640. Accessed 17 April 2023.